ASMS

RESEARCH ARTICLE

Gas-Phase Stability of Negatively Charged Organophosphate Metabolites Produced by Electrospray Ionization and Matrix-Assisted Laser Desorption/Ionization

Daiki Asakawa,[1] Hajime Mizuno,[2] Toshimasa Toyo'oka[2]

[1]National Institute of Advanced Industrial Science and Technology (AIST), Tsukuba Central 2, Umezono 1-1-1, Tsukuba, Ibaraki 305-8568, Japan
[2]Laboratory of Analytical and Bioanalytical Chemistry, School of Pharmaceutical Sciences, University of Shizuoka, 52-1 Yada, Suruga-ku, Shizuoka 422-8526, Japan
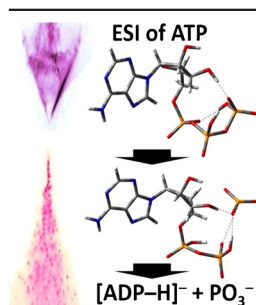
Abstract. The formation mechanisms of singly and multiply charged organophosphate metabolites by electrospray ionization (ESI) and their gas phase stabilities were investigated. Metabolites containing multiple phosphate groups, such as adenosine 5'-diphosphate (ADP), adenosine 5'-triphosphate (ATP), and D-*myo*-inositol-1,4,5-triphosphate (IP_3) were observed as doubly deprotonated ions by negative-ion ESI mass spectrometry. Organophosphates with multiple negative charges were found to be unstable and often underwent loss of PO_3^-, although singly deprotonated analytes were stable. The presence of fragments due to the loss of PO_3^- in the negative-ion ESI mass spectra could result in the misinterpretation of analytical results. In contrast to ESI, matrix-assisted laser desorption ionization (MALDI) produced singly charged organophosphate metabolites with no associated fragmentation, since the singly charged anions are stable. The stability of an organophosphate metabolite in the gas phase strongly depends on its charge state. The fragmentations of multiply charged organophosphates were also investigated in detail through density functional theory calculations.

Keywords: Charge state, Fragmentation, ADP, ATP, Density functional theory

Introduction

Electrospray ionization mass spectrometry (ESI-MS) [1] is widely used for the analysis of biomolecules. Analytes such as peptides, proteins, and nucleic acids are extracted into the gas phase as multiply charged molecules during ESI. The charge states of analytes observed by ESI mass spectrometry are strongly influenced by the chemical properties of the analyte molecules. In particular, the number of ionizable sites in the analyte is important for the charge state of the analyte observed during ESI-MS analysis. In the case of peptides, the number of protons binding to the peptide in the gas phase is similar to the number of protonation sites of the peptide in aqueous solution [2]. The properties of the solvent also affect the charge states of the peptide observed by ESI mass spectrometry [3], as ion–solvent interactions contribute to the

stabilization of the ions in solution [4, 5]. Solvents with high polarity favor analyte ions with multiple charges, probably because of their ability to efficiently solvate ions. In contrast to peptides, the charge states of protein ions observed by ESI mass spectrometry strongly depend on not only their amino acid sequence, but also their conformation. Although the ESI of protein solutions containing organic solvents and acids show broad distributions of highly charged protein ions resulting from the denaturation of proteins in solution, the use of a buffered aqueous solution for ESI avoids protein denaturation and produces narrower distributions of less-charged proteins with native-like conformation [6]. The charge states of positively and negatively charged protein ions with native-like conformation can be increased by exposure to gaseous acids and bases, respectively, through denaturation and subsequent proton transfer reactions [7, 8]. The proton-transfer reactivity of protein ions with volatile bases is influenced by the gas-phase basicities of both the protein ion and the base [9, 10]. The temperature and protein structure are also affected by the reactivity of the protein ion. Regarding the nature of the

Correspondence to: Daiki Asakawa; _e-mail:_ d.asakawa@aist.go.jp, Hajime Mizuno; _e-mail:_ hmizuno@u–shizuoka–ken.ac.jp

solvent, the surface tension of the ESI droplet is also influenced by the charge state of the protein [9, 11]. For instance, the addition of less volatile compounds such as glycerol or *m*-nitrobenzyl alcohol increases the charge state of the analyte [12–14]. This phenomenon is referred to as "supercharging" and is observed in both positive- and negative-ion modes [15]. The details of the ESI mechanism for proteins are still under investigation.

We focused on the production of multiply charged small molecules by negative-ion ESI. Recently, Ligand et al. reported that compounds are often required to have low pK_{a1} and pK_{a2} values to be observed as doubly charged molecules in negative ESI mass spectrometry [16]. Regarding the difference between ions in the gas phase and in solution, ion–solvent interactions are nonexistent in the gas phase and the lack of such interactions significantly decrease the stabilities of multiply charged molecules when the distances between the charged sites in these ions are small. Therefore, the charge state of the analyte in solution does not always correlate with the charge state observed in the ESI mass spectrum. For example, small organic dicarboxylic acids are mainly observed in their singly charged forms in their ESI mass spectra, although they have low pK_{a1} and pK_{a2} values and therefore are mostly present as dicarboxylate ions in aqueous solution [17]. The yield of the dicarboxylate ion increases with increasing carbon-backbone length, indicating that the distance between the charged sites is important for the formation of multiply charge ions by ESI [17].

In the present study, we focused on the ionization mechanisms of phosphate acid-containing metabolites, since organophosphate metabolites play important roles in a variety of biological processes. In particular, adenosine 5'-diphosphate (ADP) and adenosine 5'-triphosphate (ATP) are ubiquitous biological molecules that play essential biochemical roles, as they are the primary molecules through which energy is transported in living cells. As for small organic dicarboxylic acids, ADP and ATP are usually detected as singly and doubly deprotonated species [18], although ADP and ATP have three and four deprotonation sites, respectively. According to a previous report [19], ATP has a low pK_{a3} value and is therefore present mostly as $[ATP–3H]^{3-}$ in neutral aqueous solution. However, $[ATP–3H]^{3-}$ is barely observed in the ESI mass spectrum because of the absence of solvent interactions. Because the stabilities of multiply charged small organic compounds in the gas phase are usually low, such reductions in charge occur by proton transfer from solvent molecules during solvent evaporation. In contrast to these proton-transfer reactions, the dissociation of multiply charged molecules to produce fragment ions with fewer charges occurs by Coulombic repulsion. In the case of a peptide, collision-induced dissociation (CID) of doubly protonated peptides mainly produces singly charged product pairs [20]. Similarly, CID of $[ADP–2H]^{2-}$ and $[ATP–2H]^{2-}$ results in the dominant loss of PO_3^-, to generate singly charged fragment pairs. Importantly, these fragmentations were found to occur during ESI process; ATP and ADP produced fragment ions with *m/z* values that correspond to the deprotonated forms of ADP and 5'-adenylic acid (AMP), respectively. Consequently, these fragmentations hamper the unambiguous identification of ATP, ADP, and AMP. A deeper understanding of these ESI-induced fragmentations is necessary for the accurate identification of organophosphate metabolites. The fragmentation mechanisms of organophosphate metabolites were investigated in detail by density functional theory (DFT) calculations. The combined experimental and computational studies reveal that analytes with multiple negative charges facilitate the loss of PO_3^-, whereas singly charged analytes are stable. In order to determine the propensity of multiply charged analytes toward fragmentation, organophosphate metabolites were also analyzed by matrix-assisted laser desorption/ionization (MALDI) [21], which mainly produces singly charged analytes. Since MALDI did not produce multiply charged analytes, fragment ions resulting from bond cleavage at phosphate ester/anhydride linkages were absent in the MALDI mass spectra.

Experimental

Materials

AMP, ADP disodium salt, and ATP disodium salt were purchased from Tokyo Chemical Industry Co. (Tokyo, Japan). D-*myo*-inositol-1,4,5-triphosphate (IP$_3$) tripotassium salt, ammonium formate (HCOONH$_4$, LC-MS grade), and 9-aminoacridine (9-AA) were purchased from DOJINDO Laboratories (Kumamoto, Japan), Fisher Scientific (Fair Lawn, NJ, USA), and Sigma-Aldrich (St. Louis, MO, USA), respectively. All solvents used were of LC-MS grade, except for water, which was purified using an ultrapure water purification system (PURELAB flex, Elga, UK). The conductivity of the purified water was 18.2 MΩ/cm.

ESI-MS

Stock solutions (10 mM) of each analyte molecule (AMP, ADP, ATP, and IP$_3$) in water were prepared, and then further diluted with 3:1 (v/v) water/methanol to concentrations of 10 μM. Various amounts of ammonium formate were added to separate analyte solutions to achieve concentrations of 0–10 mM. The analyte solutions were directly injected into a triple quadrupole mass spectrometer (Xevo TQD; Waters, Milford, MA, USA) at a flow rate of 20 μL/min and ionized by a conventional ESI ion source. The capillary and cone voltages were set at 2.5 kV and 20 V, respectively, and the desolvation temperature was set at 400 °C. The desolvation and cone gas flows were set at 5.8 and 2.5 L/min, respectively. ESI mass spectra were obtained by scanning the first quadrupole filter over the 40–600 *m/z* range. For tandem mass spectrometry experiments, precursor ions were mass-selected in the first quadrupole filter, and then dissociated by CID. The CID-MS^2 mass spectra were obtained by scanning the generated fragment ions in the third quadrupole filter over the 60–600 *m/z* range. The collected data were analyzed using MassLynx software

(Waters). In order to confirm the repeatability of the results, experiments were performed more than three times under the same condition to obtain similar mass spectra. Typical ESI-MS and CID-MS^2 spectra are shown in the pertinent figures.

MALDI-MS

Solutions (25 μM) of each analyte molecule (AMP, ADP, ATP, and IP$_3$) in water were prepared. A 9-AA matrix solution was prepared at a 10 mg/mL concentration using a 1:1 (v/v) H$_2$O/acetonitrile mixture. Then, 5 μL of the analyte solution was mixed with 5 μL of the matrix solution. A total of 1 μL of the obtained mixture was deposited on a stainless steel plate, and the solvents were left to evaporate under ambient conditions. MALDI mass spectra were recorded using a MALDI-time-of-flight mass spectrometer equipped with a nitrogen laser (AXIMA-CFR Plus; Shimadzu, Kyoto, Japan). Laser power was optimized to obtain MALDI mass spectra with high ion-peak signal-to-noise ratios. The analyzer was operated in linear mode with pulsed ion extraction. Total MALDI mass spectra were obtained from 500 single spectra.

Calculations

All electron structure calculations were carried out with the Gaussian 09 program [22]. The geometries of the analytes were optimized using DFT at the M06-2X hybrid functional [23] and 6-31+G(d,p) basis set. All structures were characterized by frequency calculations to be local energy minima on their respective potential energy surfaces, and harmonic frequencies were used to determine zero-point energy corrections. To establish the energetics for the fragmentation of [ADP–2H]$^{2-}$, [ATP–2H]$^{2-}$, and [IP$_3$–3H]$^{3-}$, transition state (TS) geometries were also optimized at the M06-2X/6-31+G(d,p) level; vibrational frequency analyses exhibited only one imaginary frequency for each TS, confirming that these structures are true transition states. Selected optimized structures and their energies are shown in the pertinent schemes.

Results and Discussion

In the present study, AMP, ADP, ATP, and IP$_3$ were used as model systems to investigate the ESI ionization mechanism. Solvent pH has been reported to be an important factor that influences the yield of doubly charged ions generated by negative-ion ESI mass spectrometry; these ions were reported to be efficiently produced under alkaline conditions [16, 17]. However, organophosphate metabolites have usually been analyzed by negative-ion ESI mass spectrometry coupled with hydrophilic interaction liquid chromatography (HILIC). For HILIC-ESIMS analysis, the HCOONH$_4$ buffer was added to the analyte solution at a final concentration of 10 mM. Figure 1 displays the ESI mass spectra of the AMP, ADP, and ATP metabolites. In the spectrum of AMP (Figure 1a), a peak
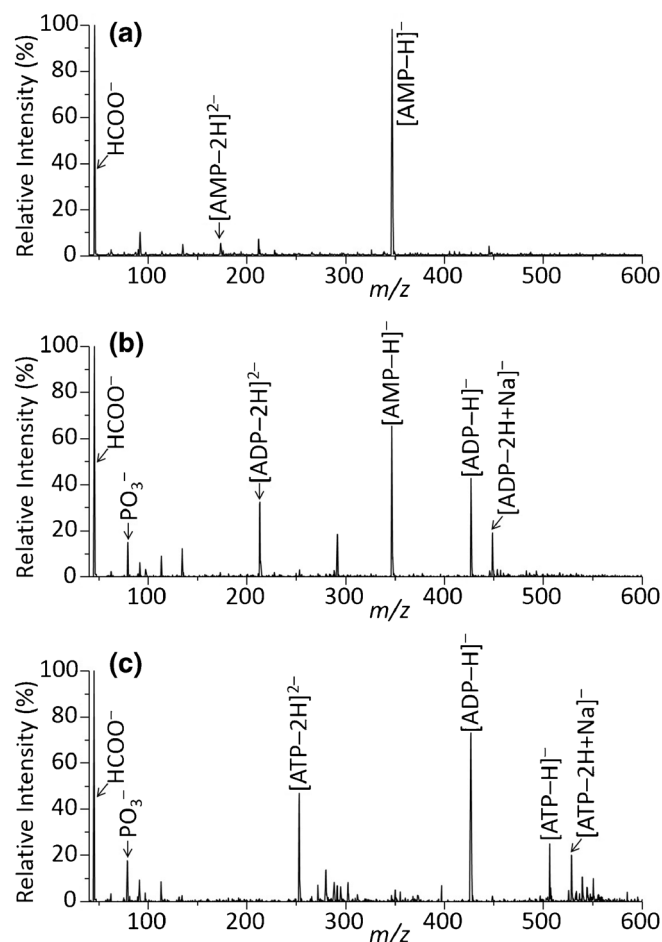

Figure 1. Negative ESI mass spectra of 10 μM **(a)** AMP, **(b)** ADP, and **(c)** ATP. The water/methanol (3/1, v/v) containing 10 mM HCOONH$_4$ was used as the solvent

corresponding to [AMP–H]$^-$ is observed to dominate, whereas ADP and ATP produced both singly and doubly deprotonated ions, as shown in Figure 1b and c. Since a compound is required to possess low pK$_{a1}$ and pK$_{a2}$ values to efficiently produce doubly charged ions in the negative ESI mass spectrum [16], we focused on the pK$_a$ values of the organophosphate metabolites. The pK$_{a1}$ and pK$_{a2}$ values of AMP are 0.9 and 3.8, respectively, whereas these values for ADP and ATP are both less than 2 [19]. As a consequence, AMP is less acidic compared with ADP and ATP, and the low yield of doubly deprotonated AMP is attributed to its higher pK$_{a2}$ value. Regarding ATP, it possesses four acidic protons, three of which have pK$_a$ values less than 2 [19]. However, [ATP–3H]$^{3-}$ was absent in its negative ion ESI mass spectrum, probably because of its low stability in the gas phase. Proton-transfer reactions between multiply charged analytes and solvent molecules are suggested to occur during solvent evaporation. Therefore, the charge-state distribution observed in the ESI mass spectrum was not directly predicted from the acidities of the analyte in solution.
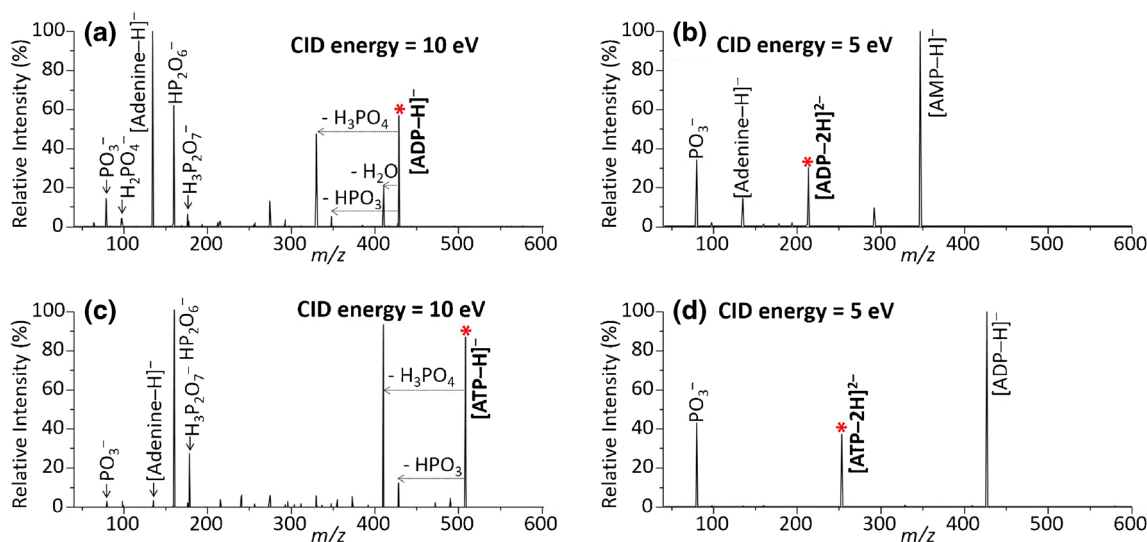
Figure 2. ESI-CID-MS^2 mass spectra of **(a)** [ADP–H]$^-$, **(b)** [ADP–2H]$^{2-}$, **(c)** [ATP–H]$^-$, and **(d)** [ATP–2H]$^{2-}$. Red asterisks indicate the precursor ions

We next focused on the fragment ions arising from the cleavage of the anhydric phosphate bonds observed in the ESI mass spectra of ADP (Figure 1b) and ATP (Figure 1c). Notably, the fragment ions generated from ADP and ATP have the same m/z values as deprotonated AMP and ADP, respectively. The presence of these fragment ions, i.e., [AMP–H]$^-$ and [ADP–H]$^-$, clearly contributes to the misinterpretation of the ESI spectra of ADP and ATP. To avoid such misinterpretations, it is important to investigate the dissociation mechanisms of the anhydric phosphate bonds in ADP and ATP. In particular, PO$_3^-$, at m/z 79, was generated from ADP and ATP as a fragment ion, whereas it was absent in the ESI mass spectrum of AMP. The results suggest that PO$_3^-$ is the

matching counterpart of the [AMP–H]$^-$ and [ADP–H]$^-$ fragment ions. In other words, these fragment ions are generated by the dissociation of the doubly deprotonated precursors, as shown in Equations 1 and 2:

$$[ADP–2H]^{2-} \rightarrow [AMP–H]^- + PO_3^- \qquad (1)$$

$$[ATP–2H]^{2-} \rightarrow [ADP–H]^- + PO_3^- \qquad (2)$$

In order to confirm these fragmentation processes, CID-MS^2 analyses of [ADP–2H]$^{2-}$ and [ATP–2H]$^{2-}$ were performed (Figure 2b and d). As expected, the [ADP–2H]$^{2-}$ and [ATP–2H]$^{2-}$ precursor ions underwent selective PO$_3^-$ loss leading to [AMP–H]$^-$ and [ADP–H]$^-$, respectively. For comparison, we also performed CID-MS^2 analyses of [ADP–H]$^-$ (Figure 2a) and [ATP–H]$^-$ (Figure 2c). The higher CID energies required for the fragmentation of the singly charged precursors indicate that [ADP–2H]$^{2-}$ and [ATP–2H]$^{2-}$ are more labile than [ADP–H]$^-$ and [ATP–H]$^-$. As shown in Figure 2a and c, the CID mass spectra of the singly charged precursors reveal the formation of a variety of fragments, such as PO$_3^-$, HP$_2$O$_6^-$, H$_3$P$_2$O$_7^-$, and [adenine–H]$^-$, and the loss of H$_3$PO$_4$ and HPO$_3$. Selective cleavage of the anhydric phosphate bond occurred when the doubly deprotonated precursor was used. Therefore, these results indicate that the [AMP–H]$^-$ and [ADP–H]$^-$ fragment ions originate from [ADP–2H]$^{2-}$ and [ATP–2H]$^{2-}$, respectively.

As described above, [AMP–H]$^-$ and [ADP–H]$^-$ are considered to be formed from [ADP–2H]$^{2-}$ and [ATP–2H]$^{2-}$, respectively, by the loss of PO$_3^-$. We next investigated the details of the fragmentation process by DFT calculations. Burke et al. reported global minimum energy conformation of [ADP–2H]$^{2-}$
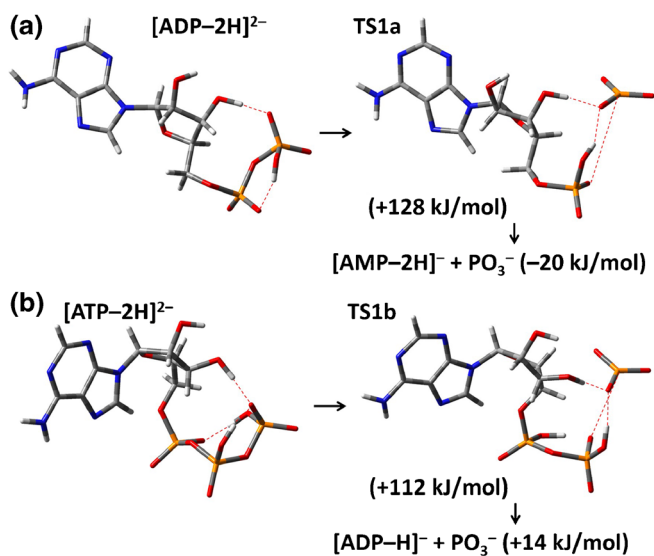
Scheme 1. Mechanism of PO$_3^-$ loss from **(a)** [ADP–2H]$^{2-}$ and **(b)** [ATP–2H]$^{2-}$. The relative energy (kJ/mol) were obtained by M06-2X/6-31+G(d,p) level calculations
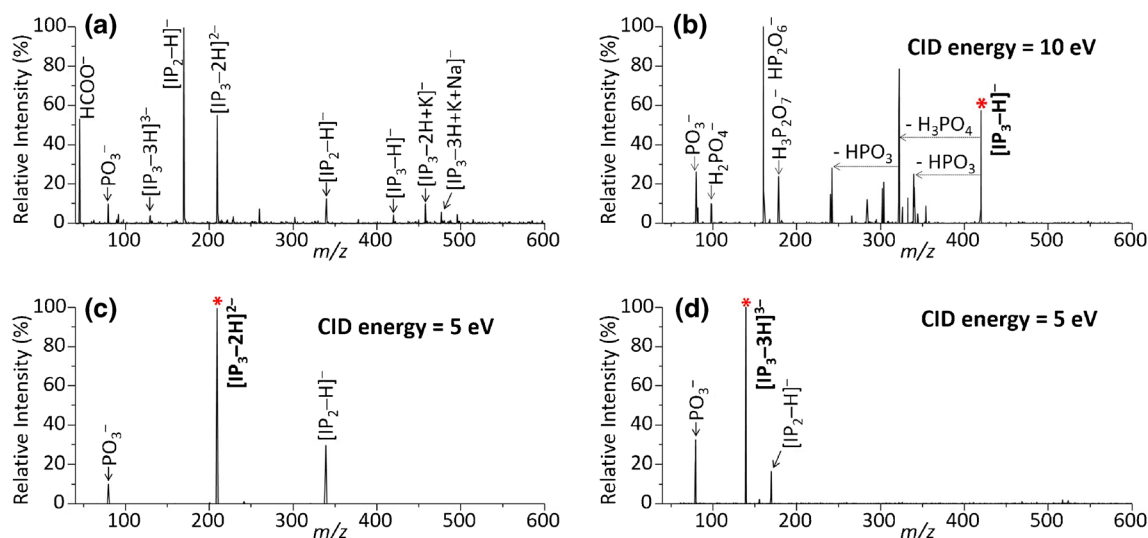
Figure 3. **(a)** Negative ESI mass spectra of 10 μM IP$_3$. The water/methanol (3/1, v/v) containing 10 mM HCOONH$_4$ was used as the solvent. **(b)–(d)** Subsequent CID-MS^2 mass spectra of **(b)** [IP$_3$–H]$^-$, **(c)** [IP$_3$–2H]$^{2-}$, and **(d)** [IP$_3$–3H]$^{3-}$. Red asterisks indicate the precursor ions

and [ATP–2H]$^{2-}$ obtained at the B3LYP/6-31+G(d) level of theory [18]. Herein we used these reported structures as the initial conformation for transition-state searching. In order to locate transition state conformation, the length of each anhydric phosphate bond was increased until an energy maximum was reached; the corresponding conformation was then further optimized to the saddle point at the M06-2X/6-31+G(d,p) level. Subsequent intrinsic reaction coordinate (IRC) analyses [24] confirmed that the optimized transition state structures are linked to the reactants. Calculated fragmentation pathways are shown in Scheme 1.

In the case of [ADP–2H]$^{2-}$, ADP possesses three deprotonation sites and two of these groups are strongly ionizable. As shown in Scheme 1a, the minimum energy conformation of [ADP–2H]$^{2-}$ is deprotonated at two phosphate residues, with the retained proton located on the terminal phosphate group. The transition state corresponding to the cleavage of the anhydric phosphate bond is shown as TS1a. Proton transfer from the terminal to the first phosphate residue occurs concomitantly with bond cleavage; TS1a was calculated to be 128 kJ/mol higher in energy than the optimized conformation of

[IP$_3$–3H]$^{3-}$ TS2

(+119 kJ/mol)

[IP$_2$–2H]$^{2-}$ + PO$_3^-$ (−213 kJ/mol)

Scheme 2. Fragmentation processes of [IP$_3$–3H]$^{3-}$. The relative energy (kJ/mol) was obtained by M06-2X/ 6-31+G(d,p) level calculations

[ADP–2H]$^{2-}$. The products, [AMP–H]$^-$ and PO$_3^-$, are more stable than [ADP–2H]$^{2-}$ by 20 kJ/mol.

Subsequently, we focused on the fragmentation of [ATP–2H]$^{2-}$ (Scheme 1b). The minimum energy conformation of [ATP–2H]$^{2-}$ is deprotonated at the first and terminal phosphate groups. Loss of PO$_3^-$ proceeds through TS1b, which is 112 kJ/mol higher in energy than the optimized conformation of [ATP–2H]$^{2-}$. As was observed for [ADP–2H]$^{2-}$, cleavage at the anhydric phosphate bond and proton transfer between the phosphate groups occur synchronously. The products, [ADP–H]$^-$ and PO$_3^-$, are less stable than [ATP–2H]$^{2-}$ by 14 kJ/mol. In summary, the barriers for PO$_3^-$ loss from [ADP–2H]$^{2-}$ and [ATP–2H]$^{2-}$ are 128 and 112 kJ/mol, respectively. The feasibility of the proposed fragmentation pathways during ESI processes is discussed below.

We next turned our attention to the examination of the ESI mass spectrum of IP$_3$, an organophosphate metabolite bearing three phosphoric acid residues (Figure 3a). Each phosphoric acid monoester possesses two acidic protons, and a proton is strongly acid. Therefore, IP$_3$ is present as [IP$_3$–3H]$^{3-}$ in neutral aqueous solution. However, the ESI mass spectrum of IP$_3$ exhibits an intense signal corresponding to [IP$_3$–2H]$^{2-}$, whereas that for [IP$_3$–3H]$^{3-}$ is weak. In addition, fragments resulting from cleavage of the phosphate ester bonds, i.e., [IP$_2$–2H]$^{2-}$ and [IP$_2$–H]$^-$, were observed in the ESI mass spectrum, as was observed for ADP and ATP. Since ions in solution phase are stabilized by ion–solvent interactions, solvent evaporation during the ESI process decreases the stability of [IP$_3$–3H]$^{3-}$. As a result, IP$_3$ reduces its charge state by proton-transfer reduction and fragmentation. Notably, fragmentation of IP$_3$ in the ESI source generates fragment ions that have the same m/z values as deprotonated inositol diphosphate, [IP$_2$–2H]$^{2-}$ and [IP$_2$–H]$^-$. As was observed for ADP and ATP, the loss of PO$_3^-$ from multiply deprotonated IP$_3$ leads to [IP$_2$–2H]$^{2-}$ and [IP$_2$–H]$^-$, which contributes to the misinterpretation of the corresponding
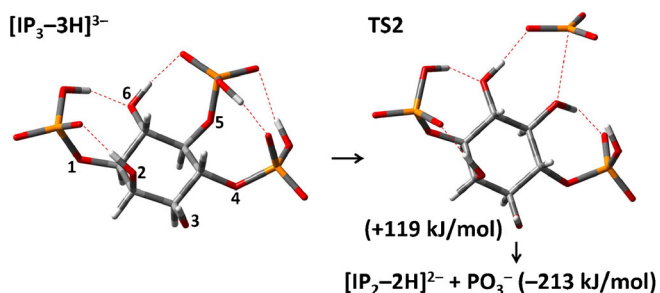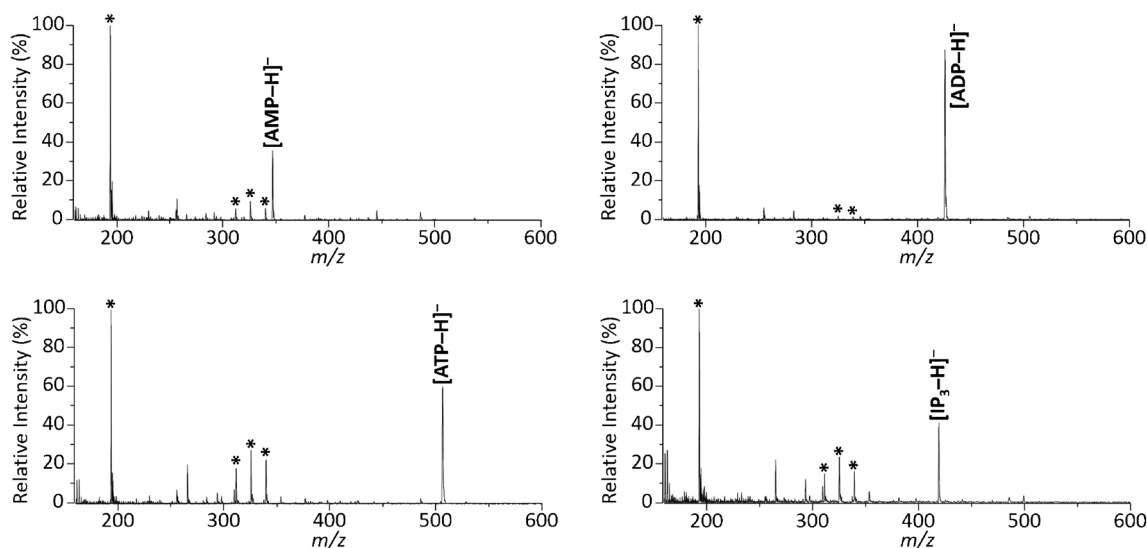
Figure 4. MALDI mass spectra of **(a)** AMP, **(b)** ADP, **(c)** ATP, and **(d)** IP$_3$. 9-Aminoacridine was used as a matrix. Asterisks indicate the signal originated from matrix

ESI mass spectra. In order to confirm the fragmentation process, we performed CID-MS^2 experiments on each charge state of deprotonated IP$_3$, i.e., [IP$_3$–H]$^-$ (Figure 3b), [IP$_3$–2H]$^{2-}$ (Figure 3c), and [IP$_3$–3H]$^{3-}$ (Figure 3d). As expected, CID of multiply charged IP$_3$, i.e., [IP$_3$–2H]$^{2-}$ and [IP$_3$–2H]$^{2-}$, revealed the formation fragment ions involving the loss of PO$_3^-$ (Figure 3c and d). In contrast, the fragmentation of singly charged IP$_3$ requires a higher CID energy compared with those of the multiply charged IP$_3$ ions, and the CID mass spectrum of the singly charged precursor exhibits a variety of fragments (Figure 3b). Therefore, the CID-MS^2 results suggest that the intense signal corresponding to doubly deprotonated IP$_2$, [IP$_2$–2H]$^{2-}$, is formed through the loss of PO$_3^-$ from [IP$_3$–3H]$^{3-}$ during the ESI process.

The fragmentation mechanism was subsequently investigated using DFT calculations, and the proposed pathway is shown in Scheme 2. IP$_3$ bears three phosphate groups and each phosphoric acid monoester possesses a strongly acidic proton. As expected, the calculations reveal that each phosphate group bears a single negative charge in the minimum energy conformation of [IP$_3$–3H]$^{3-}$. The negatively charged phosphate groups in [IP$_3$–3H]$^{3-}$ are stabilized by intramolecular hydrogen bonding to either hydroxyl or neighboring phosphate groups. In order to locate the global minimum-energy structure, we searched for the [IP$_3$–3H]$^{3-}$ conformation with the maximum number of intramolecular hydrogen bonds. Scheme 2 displays the optimized minimum-energy structure of [IP$_3$–3H]$^{3-}$, which was then used as the initial conformation for the location of the transition state for the loss of PO$_3^-$. As illustrated in Scheme 2, phosphate groups are located at positions 1, 4, and 5 in IP$_3$. Upon fragmentation, a phosphate ester bond in [IP$_3$–3H]$^{3-}$ is cleaved to yield the HPO$_3$ and [IP$_2$–3H]$^{3-}$ fragment pair. In order to form PO$_3^-$ and [IP$_2$–2H]$^{2-}$, a proton must concurrently be transferred from HPO$_3$ to [IP$_2$–3H]$^{3-}$ during bond cleavage.

The negatively charged phosphate group is the most probable site for proton accepter. Since the phosphate groups at positions 4 and 5 are bound through hydrogen bonds, bond cleavage and proton transfer occur concurrently when the phosphate ester bonds at positions 4 or 5 are cleaved. As a result, the fragment ion, [IP$_2$–2H]$^{2-}$, is generated as an alkoxide-bearing compound, and proton transfer from the phosphate moiety to the alkoxide occurs because of the low stability of the alkoxide group. According to the consideration of stereochemistry considered, proton transfer from the phosphate moiety to the alkoxide is possible when the phosphate bond at position 5 is cleaved. Consequently, the cleavage of the phosphate bond at position 5 proceeds since it follows a lower-energy pathway compared with those for phosphate bond cleavage at positions 1 and 4. Therefore, we propose that the PO$_3^-$ originates from the phosphate group at position 5. The calculated fragmentation pathway is illustrated in Scheme 2. The loss of PO$_3^-$ from [IP$_3$–3H]$^{3-}$ proceeds through transition state, TS2, which is calculated to lie 119 kJ/mol higher in energy than the optimized conformation of [IP$_3$–3H]$^{3-}$. The products, [IP$_2$–2H]$^{2-}$ and PO$_3^-$, are more stable than [IP$_3$–3H]$^{3-}$ by 213 kJ/mol. The energy barrier for the loss of PO$_3^-$ from [IP$_3$–3H]$^{3-}$ is comparable to those calculated for the similar fragmentations from [ADP–2H]$^{2-}$ and [ATP–2H]$^{2-}$.

We now focus on the internal energies of the ions generated by ESI, which were investigated using the survival-yield method and the benzylpyridinium "thermometer" ion [25–28]. According to previous investigations, ions formed during the course of the ESI process are significantly heated in the atmospheric pressure region, probably because of friction between the fast-moving charged droplets and the gas molecules. Subsequently, the generated gaseous ions are introduced into the vacuum through an orifice and then accelerated by the potential

deference between the orifice and the skimmer. As a result, collisions between the analyte ions and the gas also increase the internal energies of the ions. Although this effect depends greatly on the source design, acceleration potential, and the nature of the collision gas used, among other factors [25–28], the internal energies of the ions produced by ESI are estimated to be around 180 kJ/mol when standard parameter sets and the benzylpyridinium "thermometer" ion are used. The organophosphate metabolites are larger than benzylpyridinium and their internal energies depend on their degrees of freedom. Briefly, a relatively large organophosphate metabolite requires more energy to increase its internal temperature by the same amount as the relatively small benzylpyridinium "thermometer" ion. As depicted in Schemes 1 and 2, the energy barriers for the loss of PO_3^- from $[ADP–2H]^{2-}$, $[ATP–2H]^{2-}$, and $[IP_3–3H]^{3-}$ are around 120 kJ/mol. Although the internal energies of benzylpyridinium and the organophosphate metabolites are not compared directly, the proposed fragmentation pathways are regarded to be feasible for ESI processes.

The ESI operating low temperature has been developed in order to obtain analyte-ion information in the solution phase [29, 30]. In this case, the internal energy of the system before ionization is minimized, allowing for the detection of fragile non-covalent assemblies. The cooling of the ESI source may allow the detection of organophosphate metabolites as the intact form. However, these experimental conditions sometimes provide partially solvated analyte ions [30], which are detrimental to the analytical procedure.

For comparison, AMP, ADP, ATP, and IP$_3$ were analyzed by MALDI-MS (Figure 4). Since 9-AA has been reported to be an effective matrix in negative-mode MALDI experiments [31], it was also used in our experiments. As shown in Figure 4, all analytes were detected as singly deprotonated form, $[M–H]^-$; notably, multiply charged species were absent in the MALDI mass spectra. Importantly, no fragment ions resulting from the cleavage of phosphate ester/anhydride bonds were observed in the MALDI mass spectra. Although the internal energies of the analyte ions generated by MALDI using benzylpyridinium "thermometer" ion were about 300 kJ/mol [32, 33], which is ~120 kJ/mol higher than those generated by ESI, the MALDI technique did not facilitate fragmentation. Such a phenomenon is probably the result of the high stabilities of the singly charged analytes, confirming that the stability of an analyte ion is strongly related to its charge state. Notably, the organophosphate metabolites induced by analyte fragmentation during ESI that result in the formation of multiply charged analytes contribute to the misinterpretation of the ESI spectra of these species. In contrast, MALDI produces singly charged molecules without any fragmentation, providing accurate information for the identification of organophosphate metabolites.

Conclusion

In order to investigate the details of ESI fragmentation mechanisms, we used the AMP, ADP, ATP, and IP$_3$ organophosphate metabolites as model systems. The ESI of these metabolites gave mainly singly and doubly charged species, and the fragmentation processes depended on the charge state. Although singly charged organophosphate anions were found to be stable, organophosphates with multiple negative charges often underwent PO_3^- loss. Therefore, the ESI mass spectra of ADP, ATP, and IP$_3$ exhibit fragment ions, $[AMP–H]^-$, $[ADP–H]^-$, and $[IP_2–2H]^{2-}$, respectively. According to DFT calculations, energy barriers for the loss of PO_3^- from multiply charged organophosphate metabolites are around 120 kJ/mol. Since the internal energies of the ions produced by ESI with standard parameter sets is estimated to be around 180 kJ/mol, the proposed ESI fragmentation pathway is feasible. As a consequence, these fragment ions contribute to the misinterpretation of the corresponding ESI mass spectra. In order to unambiguously identify organophosphates, ESI-MS should be combined with chromatographic techniques, with each organophosphate metabolite separated from the other components before ESI-MS analysis. In contrast to ESI, MALDI produced singly charged organophosphate metabolites with no fragmentation. Therefore, MALDI-MS can be used for the direct identification of organophosphate metabolites.

Acknowledgements

References

1. Fenn, J.B., Mann, M., Meng, C.K., Wong, S.F., Whitehouse, C.M.: Electrospray ionization for mass spectrometry of large biomolecules. Science. **246**, 64–71 (1989)

2. Smith, R.D., Loo, J.A., Loo, R.R.O., Busman, M., Udseth, H.R.: Principles and practice of electrospray ionization-mass spectrometry for large polypeptides and proteins. Mass Spectrom. Rev. **10**, 359–452 (1991)

3. Wang, G., Cole, R.B.: Effects of solvent and counterion on ion pairing and observed charge state of diquaternary ammonium salts in electrospray ionization mass spectrometry. J. Am. Soc. Mass Spectrom. **7**, 1050–1058 (1996)

4. Ding, C.-F., Wang, X.-B., Wang, L.-S.: Photoelectron spectroscopy of doubly charged anions: intramolecular Coulomb repulsion and solvent stabilization. J. Phys. Chem. A. **102**, 8633–8636 (1998)

5. Wang, L.-S., Ding, C.-F., Wang, X.-B., Nicholas, J.B.: Probing the potential barriers and intramolecular electrostatic interactions in free doubly charged anions. Phys. Rev. Lett. **81**, 2667–2670 (1998)

6. Chowdhury, S.K., Katta, V., Chait, B.T.: Probing conformational changes in proteins by mass spectrometry. J. Am. Chem. Soc. **112**, 9012–9013 (1990)

7. Kharlamova, A., Prentice, B.M., Huang, T.-Y., McLuckey, S.A.: Electrospray droplet exposure to gaseous acids for the manipulation of protein charge state distributions. Anal. Chem. **82**, 7422–7429 (2010)

8. Kharlamova, A., McLuckey, S.A.: Negative electrospray droplet exposure to gaseous bases for the manipulation of protein charge state distributions. Anal. Chem. **83**, 431–437 (2011)

9. Gross, D.S., Schnier, P.D., Rodriguez-Cruz, S.E., Fagerquist, C.K., Williams, E.R.: Conformations and folding of lysozyme ions in vacuo. Proc. Natl. Acad. Sci. USA. **93**, 3143–3148 (1996)

10. Susa, A.C., Xia, Z., Tang, H.Y., Tainer, J.A., Williams, E.R.: Charging of proteins in native mass spectrometry. J. Am. Soc. Mass Spectrom. **28**, 332–340 (2017)

11. Loo, R.R.O., Smith, R.D.: Investigation of the gas-phase structure of electrosprayed proteins using ion-molecule reactions. J. Am. Soc. Mass Spectrom. **5**, 207–220 (1994)

12. Iavarone, A.T., Jurchen, J.C., Williams, E.R.: Effects of solvent on the maximum charge state and charge state distribution of protein ions produced by electrospray ionization. J. Am. Soc. Mass Spectrom. **11**, 976–985 (2000)

13. Iavarone, A.T., Jurchen, J.C., Williams, E.R.: Supercharged protein and peptide ions formed by electrospray ionization. Anal. Chem. **73**, 1455–1460 (2001)

14. Iavarone, A.T., Williams, E.R.: Mechanism of charging and supercharging molecules in electrospray ionization. J. Am. Chem. Soc. **125**, 2319–2327 (2003)

15. Brahim, B., Alves, S., Cole, R.B., Tabet, J.C.: Charge enhancement of single-stranded DNA in negative electrospray ionization using the supercharging reagent meta-nitrobenzyl alcohol. J. Am. Soc. Mass Spectrom. **24**, 1988–1996 (2013)

16. Liigand, P., Kaupmees, K., Kruve, A.: Ionization efficiency of doubly charged ions formed from polyprotic acids in electrospray negative mode. J. Am. Soc. Mass Spectrom. **27**, 1211–1218 (2016)

17. Dong, Y., Guella, G., Mattivi, F., Franceschi, P.: High production of small organic dicarboxylate dianions by DESI and ESI. J. Am. Soc. Mass Spectrom. **26**, 386–389 (2015)

18. Burke, R.M., Pearce, J.K., Boxford, W.E., Bruckmann, A., Dessent, C.E.H.: Stabilization of excess charge in isolated adenosine 5'-triphosphate and adenosine 5'-diphosphate multiply and singly charged anions. J. Phys. Chem. A. **109**, 9775–9785 (2005)

19. Alberty, R.A., Smith, R.M., Bock, R.M.: The apparent ionization constants of the adenosinephosphates and related compounds. J. Biol. Chem. **193**, 425–434 (1951)

20. Harrison, A.G.: Charge-separation reactions of doubly protonated peptides: effect of peptide chain length. J. Am. Soc. Mass Spectrom. **20**, 1890–1895 (2009)

21. Karas, M., Hillenkamp, F.: Laser desorption ionization of protein with molecular masses exceeding 10,000 daltons. Anal. Chem. **60**, 2299–2301 (1988)

22. Frisch, M.J., Trucks, G.W., Schlegel, H.B., Scuseria, G.E., Robb, M.A., Cheeseman, J.R., Scalmani, G., Barone, V., Mennucci, B., Petersson, G.A., Nakatsuji, H., Caricato, M., Li, X., Hratchian, H.P., Izmaylov, A.F., Bloino, J., Zheng, G., Sonnenberg, J.L., Hada, M., Ehara, M., Toyota, K., Fukuda, R., Hasegawa, J., Ishida, M., Nakajima, T., Honda, Y., Kitao, O., Nakai, H., Vreven, T., Montgomery, J.A. Jr., Peralta, J.E., Ogliaro, F., Bearpark, M., Heyd, J.J., Brothers, E., Kudin, K.N., Staroverov, V.N., Keith, T., Kobayashi, R., Normand, J., Raghavachari, K., Rendell, A., Burant, J.C., Iyengar, S.S., Tomasi, J., Cossi, M., Rega, N., Millam, J.M., Klene, M., Knox, J.E., Cross, J.B., Bakken, V., Adamo, C., Jaramillo, J., Gomperts, R., Stratmann, R.E., Yazyev, O., Austin, A.J., Cammi, R., Pomelli, C., Ochterski, J.W., Martin, R.L., Morokuma, K., Zakrzewski, V.G., Voth, G.A., Salvador, P., Dannenberg, J.J., Dapprich, S., Daniels, A.D., Farkas, O., Foresman, J.B., Ortiz, J.V., Cioslowski, J., Fox, D.J.: Gaussian 09; Rev. D.01; Gaussian, Inc.: Wallingford (2010)

23. Zhao, Y., Truhlar, D.G.: The M06 Suite of Density Functionals for main group thermochemistry, thermochemical kinetics, noncovalent interactions, excited states, and transition elements: two new functionals and systematic testing of four M06-class functionals and 12 other functionals. Theor. Chem. Acc. **120**, 215–241 (2008)

24. Fukui, K.: The path of chemical reactions–the IRC approach. Acc. Chem. Res. **14**, 363–368 (1981)

25. Collette, C., De Pauw, E.: Calibration of the internal energy distribution of ions produced by electrospray. Rapid Commun. Mass Spectrom. **12**, 165–170 (1998)

26. Collette, C., Drahos, L., De Pauw, E., Vékey, K.: Comparison of the Internal energy distributions of ions produced by different electrospray sources. Rapid Commun. Mass Spectrom. **12**, 1673–1678 (1998)

27. Drahos, L., Heeren, R.M., Collette, C., De Pauw, E., Vekey, K.: Thermal energy distribution observed in electrospray ionizationy. J. Mass Spectrom. **34**, 1373–1379 (1999)

28. Gabelica, V., De Pauw, E.: Internal energy and fragmentation of ions produced in electrospray sources. Mass Spectrom. Rev. **24**, 566–587 (2005)

29. Lee, S.-W., Freivogel, P., Schindler, T., Beauchamp, J.L.: Freeze-dried biomolecules: FT-ICR studies of the specific solvation of functional groups and clathrate formation observed by the slow evaporation of water from hydrated peptides and model compounds in the gas phase. J. Am. Chem. Soc. **120**, 11758–11765 (1998)

30. Yamaguchi, K.: Cold-spray ionization mass spectrometry: principle and applications. J. Mass Spectrom. **38**, 473–490 (2003)

31. Vermillion-Salsbury, R.L., Hercules, D.M.: 9-Aminoacridine as a matrix for negative mode matrix-assisted laser desorption/ionization. Rapid Commun. Mass Spectrom. **16**, 1575–1581 (2002)

32. Luo, G., Marginean, I., Vertes, A.: Internal energy of ions generated by matrix-assisted laser desorption/ionization. Anal. Chem. **74**, 6185–6190 (2002)

33. Gabelica, V., Schulz, E., Karas, M.: Internal energy build-up in matrix-assisted laser desorption/ionization. J. Mass Spectrom. **39**, 579–593 (2004)